Contents lists available at ScienceDirect

Radiotherapy and Oncology

journal homepage: www.thegreenjournal.com

Original Article

Assessment of residual geometrical errors of clinical target volumes and their impact on dose accumulation for head and neck radiotherapy

Kelvin Ng Wei Siang [a,b,c,*], Stefan Both [a], Edwin Oldehinkel [a], Johannes A. Langendijk [a], Dirk Wagenaar [a]

[a] Department of Radiation Oncology, University Medical Center Groningen, University of Groningen; [b] Erasmus MC Cancer Institute, University Medical Center Rotterdam, Department of Radiotherapy, The Netherlands; [c] Holland Proton Therapy Center, Department of Medical Physics & Informatics, Delft, The Netherlands

ABSTRACT

Purpose: To assess the residual geometrical errors (dr) and their impact on the clinical target volumes (CTV) dose coverage for head and neck cancer (HNC) proton therapy patients.
Methods: We analysed 28 HNC patients treated with 70 Gy (RBE) and 54.25 Gy (RBE) to the therapeutic CTV_{70} and prophylactic $CTV_{54.25}$, respectively. Daily cone beam CTs were converted to high quality synthetic CTs (sCTs). The CTVs from the nominal CT were propagated to the corresponding sCTs using a hybrid deformable image registration (propagated CTVs) in RayStation 11B. For 11 patients, all propagated CTVs were reviewed by our HNC radiation oncologist (physician corrected CTVs).

The residual geometrical error dr was quantified as a function of the daily CTVs volume overlap with the nominal plan CTV. The errors dr(propagated CTVs) and dr(physician corrected CTVs) and the difference in dice similarity coefficients (ΔDSC) were determined. Using clinical plans, dose coverage and the tumor control probability (TCP) for the nominal, accumulated and voxel-wise minimum scenarios were determined.
Results: The difference in the residual geometrical error dr (propagated CTVs – physician corrected CTVs) and mean DSC ($|\Delta$DSC$|$mean) were minor: Δdr(CTV_{70}) = 0.16 mm, Δdr($CTV_{54.25}$) = 0.26 mm, $|\Delta$DSC$|$ mean < 0.9%. For all 28 patients, dr(CTV_{70}) = 1.91 mm and dr($CTV_{54.25}$) = 1.90 mm. However, $CTV_{54.25}$ above and below the cricoid cartilage differed substantially (1.00 mm c.f. 3.93 mm). The $CTV_{54.25}$ coverage below the cricoid was then almost always lower, although the TCP of the accumulated dose was higher than the TCP of the voxel-wise minimum dose.
Conclusions: Setup uncertainty setting of 2 mm is possible. The feasibility of using propagated CTVs for error determination is demonstrated.

Radiotherapy plays a pivotal role in the management of head and neck cancer (HNC) patients [1,2]. Prescription doses ranging from 54 to 70 Gy are often administered to the prophylactic and therapeutic target volumes, respectively using fractions of up to 2 Gy, 5 times/week [3]. Delivering adequate dose to the target volume is crucial to minimize locoregional recurrences [4]. To reduce dose uncertainties, anatomical and treatment setup errors should be considered in treatment planning [5,6].

Head and neck radiotherapy treatment setup is improved by performing online verification using daily cone-beam computed tomography (CBCT) on patients immobilized using thermoplastic masks and individualized head support [7,8]. However, non-rigid geometrical errors due to anatomical changes (e.g., tumor shrinkage, edema, swallowing) remain largely uncorrected [9,10], impacting target dose coverage [11], if no plan adaption is made. Target volumes can also deform independently of the head and neck anatomy [12]. Error margins due to intrafraction tumor motion in the head and neck regions are found to be negligible when excluding tongue displacements and swallowing effects (~0.2 mm) [9]. When these effects are included, the motion of tumors in the neck regions can increase up to a few millimeters [9,12]. However, the impact of swallowing on dose coverage is generally small and may be considered negligible for most patients [9,13].

Planning strategies to account for the residual geometrical errors include clinical target volume (CTV) expansion to form the planning target volume (PTV) [14,15] or scenario-based composite min–max robustness optimization (CMRO) [16,17]. With improved computational power, CMRO is becoming increasingly integrated into treatment planning for both proton and photon RT [17–19]. Unlike the PTV recipe, this method does not assume dose-error

* Corresponding author at: Erasmus University Medical Center, Department of Radiotherapy – Medical Physics and Instrumentation, Postbus 2040 3000 CA, Rotterdam, The Netherlands.
E-mail address: K.NgWeiSiang@erasmusmc.nl (K. Ng Wei Siang).

invariance [20] and accounts for range errors inherent to proton RT [17].

The use of larger CMRO setup and range uncertainty margins can increase plan robustness but comes at the cost of higher dose exposure to the organs at risk [21–23]: approximately 1 Gy/mm geometrical and 0.5 Gy/1% range uncertainty [24,25]. Robust optimization setup margins of 3 mm and up to 5 mm in the lymph nodes, the parotid glands, and the larynx regions for HNC patients immobilized with a mask and head rest have shown to be adequate for CTV dose coverage based on realistic simulated error scenarios [26,27]. With 3 mm margins, acute and late toxicity incidences were further reduced without compromising locoregional control [28]. Wagenaar et al. [25] used probabilistic dose accumulation [29] and found sufficient target coverage with 2 mm/3% geometrical and range uncertainty settings for intensity modulated proton therapy (IMPT). However, to define and validate robust geometrical uncertainty margins of 2 mm, knowledge of the residual non-rigid anatomical variations is required [30,31].

The aim of this study was to quantify the residual geometrical errors of the head and neck CTVs to determine the CMRO setup uncertainty setting. Range errors were considered 3%. Geometrical errors here include non-rigid setup errors, tumor size and shape changes and organ deformation and motion [32]. Daily synthetic CTs (sCT) corrected from CBCTs are used to assess the CTV contour variations. The impact of the errors on the accumulated dose and tumor control probability (TCP) [33] of clinically delivered plans are subsequently examined.

Materials and methods

Study cohort and treatment

In this retrospective study, 42 consecutive HNC patients treated with IMPT between December 2018 and June 2019 at our institute were included. For each patient, a daily CBCT based sCT was generated and evaluated by our HNC radiation oncologist from image quality point of view. Consequently, 14 patients were excluded from our analysis due to presence of strong dental artefacts in the CBCT scans (10) and/or insufficient CBCT field of view (4): the resulting sCTs were inadequate for the purpose of our study. As a result, our analysis was performed on 28 patients. Our patient population and the treatment characteristics are described in Supplementary, Table 1.

All HNC patients were treated using simultaneous integrated boost with 70 Gy (RBE) and 54.25 Gy (RBE) to the therapeutic CTV (CTV_{70}) and prophylactic CTV ($CTV_{54.25}$), respectively with IMPT. A constant relative biological effectiveness (RBE) factor of 1.1 was used. The IMPT beam arrangement comprises typically of four beams depending on the location of the tumor, organs at risk and the air cavities, with typical beam angles of 200°, 320°, 40° and 160° (plus a range shifter for the shallow part of the tumor [34]). Beam angle deviations of ± 20° are accepted. The beam arrangements were chosen so to avoid regions expected to be less reproducible and that the beam path in the body is as short as possible. The posterior beams were blocked from going through the shoulders expanded by a margin of 1 to 2 cm. Patients were adjusted to not have heavy skin folds in the neck area at the moulddroom, CT scanning and treatment. The anterior fields were also blocked at the sinus cavities and dental fillings. Two additional near lateral fields on top of the standard four fields were then typically included for nasopharyngeal cancers. This will avoid most of the dose contribution to the CTV_{70} from the posterior beams, which will undesirably increase the doses in brain and other healthy tissues. Patients were positioned on top of a 6D robotic couch capable of translational and rotational corrections (Leoni CIA, France) and immobilized using a 5-point mask (Orfit Indus-

tries, Belgium) to include the shoulders. For cancers of the oral cavity, e.g., tongue and floor of the mouth, a bite block or tongue depressor were also used to increase reproducibility. Before every treatment fraction, online verification was performed by rigidly registering the CBCT images to the planning CT used for treatment planning. Rigid 6D couch corrections were applied, and the treatment was delivered. Weekly verification CTs were acquired for monitoring anatomical changes, and if needed, used for plan adaptation.

To perform rigid registration between the CBCT and planning CT images, a verification box region was first defined that included all the CTVs and some of the anatomy such as the skull and mouth cavity and spine. After the patient was positioned on the table, 2D kV orthogonal images were taken and the patient was manually repositioned. After the patient adjustment was accepted, a CBCT was next acquired and an automatic match was performed in adaPT insight (IBA, Belgium) to rigidly register the CBCT and the planning CT, with the focus on the structures in the verification box. If the match is rejected upon evaluation by our radiation therapists, manual adjustments of the match would take place. The registration of the CTV_{70} and its surroundings were prioritized over the matching of $CTV_{54.25}$ and other anatomy, unless there were important OARs to be avoided.

Synthetic CTs and contour preparation

To improve the Houndsfield unit accuracy and soft tissue contrast of the CBCTs [35], the daily CBCTs were converted to high quality sCTs having a resolution of $1.0 \times 1.5 \times 2.0$ mm^3 using an in-house validated deep convolutional neural network (DCNN) architecture [36]. Our CBCTs were acquired at 100kVp and 160 mA, with a resolution = $0.5 \times 0.5 \times 2.5$ mm^3. An example of a CBCT and the corresponding sCT are displayed in Fig. 1a and b. The window width of the CBCT was set twice higher than the sCT so that the CBCT becomes visible. Visually, the sCT generated from the CBCT from the deep learning network has reduced noise, higher contrast and signal that appears more familiar to the radiation oncologist. Anatomical structures are also more visible on the sCT compared with the CBCT. The field of view (FoV) of the CBCT was typically smaller than the FoV of the nominal plan CT. In our clinic, the CBCTs were acquired such that the CTVs were sufficiently far from the FoV edges to ensure good rigid registration between the treatment position and nominal plan CT.

The number of CBCTs (hence sCTs) images available per patient ranged from 31 to 35 (median 34). The median treatment duration was 48 days and 41 days for conventional and accelerated fractionation schedules, respectively. For every patient, the CTV contours on the nominal plan CT were propagated to the sCTs using a hybrid deformable image registration (DIR) [37] in RayStation 11B (RaySearch Laboratories, Sweden), resulting in propagated CTVs. The nominal plan CTVs (CTV_{70} and $CTV_{54.25}$) for both original and adapted (8/28 patients) plans were considered in the analysis. Of the eight patients, three had target volume contour increase due to edema, two had swelling in the beam path, one had target volume contour shrinkage due to weight loss and two had a new mask made for better position verification.

Error determination

Here, we defined the residual geometrical error dr as a function of the daily CTV volume overlap with the nominal plan CTV used for planning. The residual geometrical error dr reflects the inclusiveness index concept [38] and may be interpreted as the inclusiveness distance, or the smallest margin required to include a desired percentage of the daily CTV volume within the nominal plan CTV.
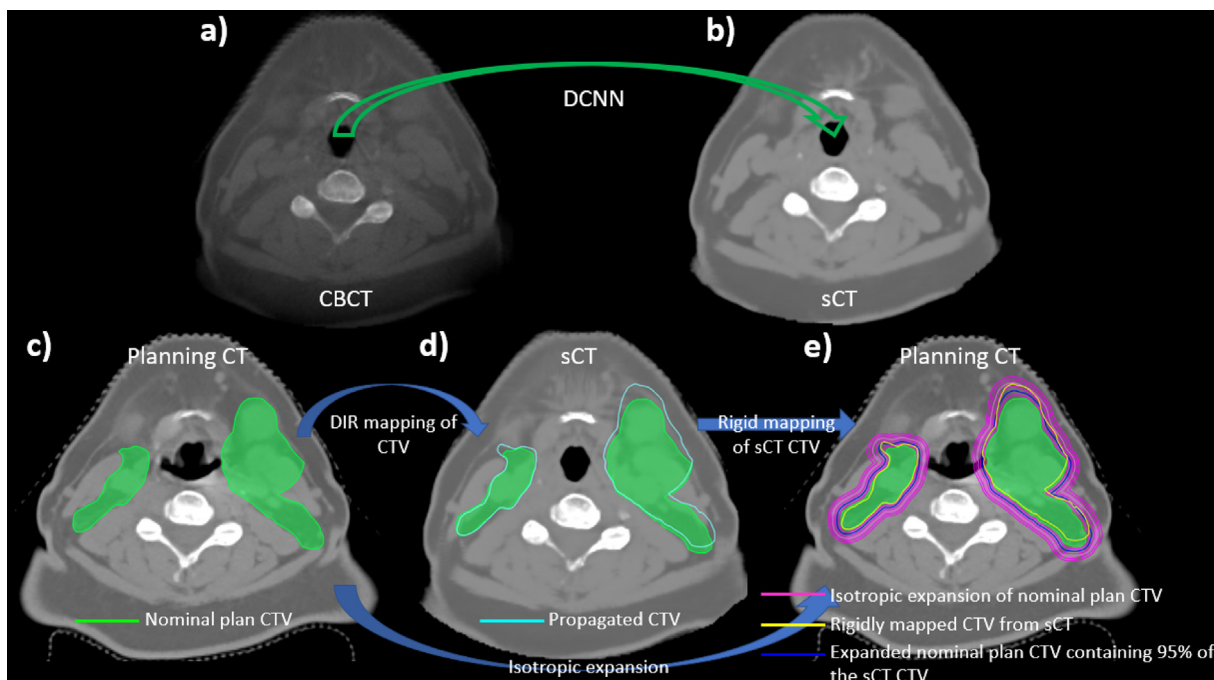
Fig. 1. Example of a (a) CBCT converted using our in-house deep convolution neural network (DCNN) to give a (b) sCT. The window width is set twice higher for the CBCT than the sCT to increase the visibility of the CBCT. Method of determining residual geometrical errors by: (c) deformably mapping the nominal plan CTV (green) to the sCT to generate the propagated CTV, d) rigidly mapping the propagated CTV (cyan) back to the nominal plan CT determining the sCT CTV and e) intersecting the rigidly mapped sCT CTV (yellow) with the expanded nominal plan CTV (pink). The expanded nominal plan CTV containing 95% of the rigidly mapped CTV is outlined in blue.
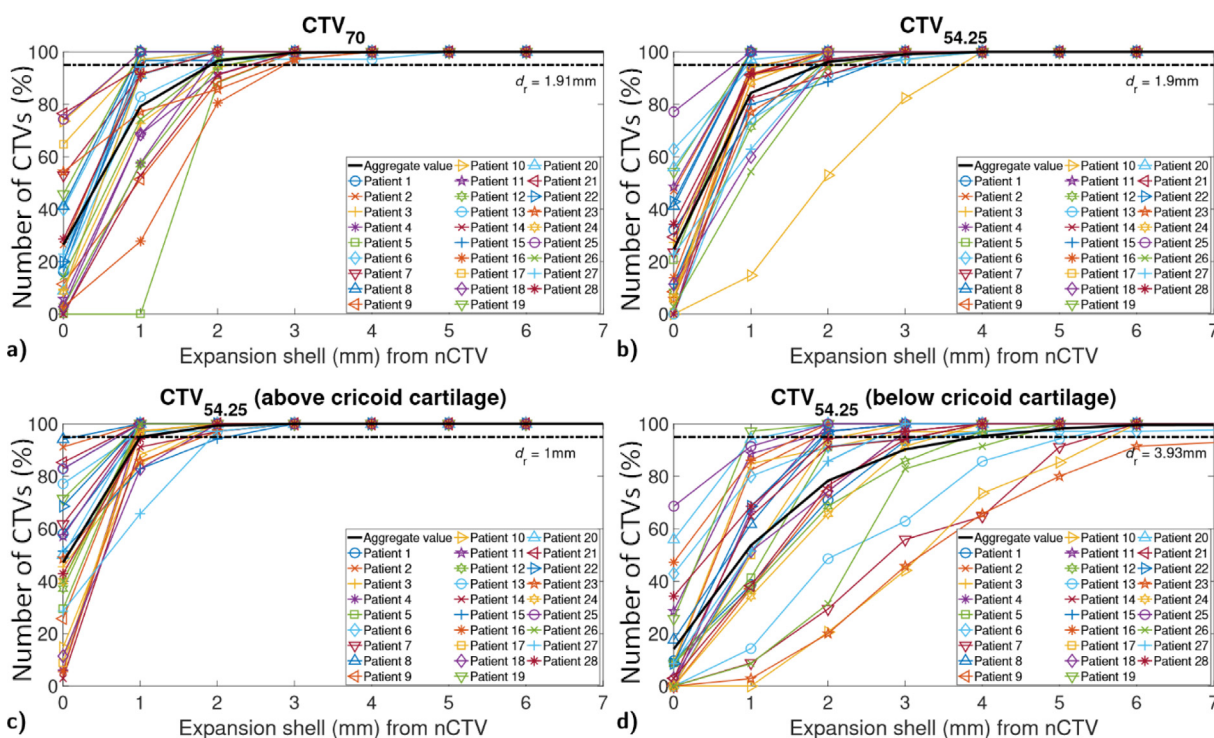

Fig. 2. Number of daily sCT CTVs (in %) against the expansion (in mm) of the nominal plan CTV for (a) CTV_{70}, (b) $CTV_{54.25}$ and $CTV_{54.25}$ regions (c) above and (d) below the cricoid cartilage for each patient and for the population (solid black line). Each marker represents the number of daily CTVs having 98% (CTV_{70}) or 95% (prophylactic $CTV_{54.25}$) volume overlap with the nominal plan CTV expanded by a certain distance for each patient. The result for the entire patient cohort is plotted as a solid black line. The horizontal dashed black line is the aggregate residual geometrical error dr.

The method to determine the residual geometrical error dr is schematically depicted in Fig. 1. After deformably mapping the nominal plan CTVs to the daily sCTs giving propagated CTVs (Fig. 1a, b), the daily propagated CTVs were rigidly mapped to the co-registered nominal plan CT (Fig. 1b, c). The nominal plan CTVs were then expanded isotropically in discrete steps of 1 mm, up to 6 mm (Fig. 1c). An extra 12 mm shell was included to capture any outliers. The rigidly mapped propagated CTVs were then inter-
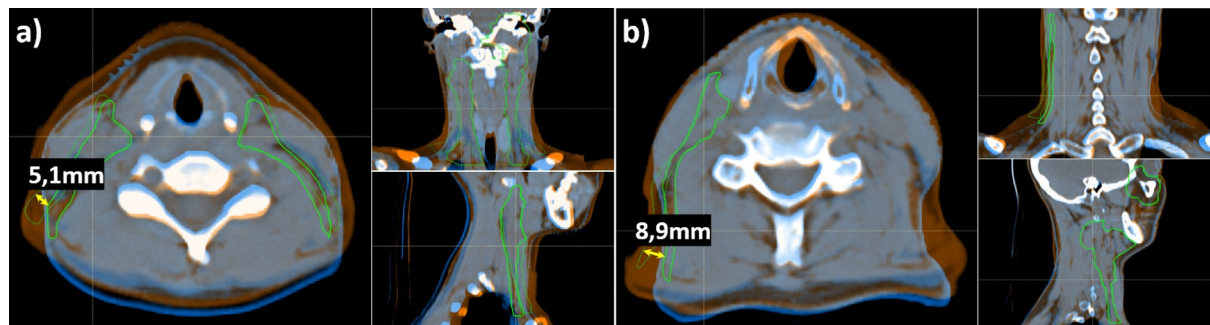
Fig. 3. The fused sCT (orange) and nominal CT (blue) scans for patients a) 10 and b) 23. The 2D axial (left), coronal (top right) and sagittal (bottom right) slices are shown, with the dotted cross hairs indicating the slice location. The axial slice is located right below the plane where $CTV_{54.25}$ is divided. The estimated magnitude of the error is displayed on the axial slice. The green solid and dotted line represents the $CTV_{54.25}$ contour on the nominal plan CT and sCT, respectively. Majority of the errors are found in the $CTV_{54.25}$ region below the cricoid cartilage, whereas the match was almost perfect in the head and upper neck region. For patient 10, 25, 5% of the $CTV_{54.25}$ volume laid below the cricoid cartilage, corresponding to the overall large residual error d_r observed in Fig. 2b. For patient 23, only 7.9% of the $CTV_{54.25}$ volume laid below the cricoid cartilage, which explains why dr of the entire $CTV_{54.25}$ was still small despite the large dr below the cricoid.
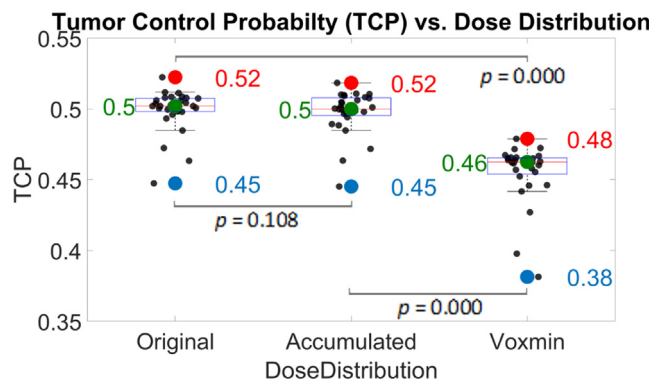
Fig. 4. Calculated TCP values for the various dose distributions. The maximum, median and minimum TCP values are indicated by the red, green and blue dots, respectively. Each black dot represents the TCP per patient.

sected with the expanded nominal plan CTVs to determine the volume overlap. For the CTV_{70}, the residual geometrical error dr was the minimum interpolated shell distance at which 95% of the daily CTVs have at least 98% volume overlap with the nominal plan CTV + dr. For the $CTV_{54.25}$ contours, the residual geometrical error dr was determined at 95% volume overlap. These percentages were defined upon consultation with our HNC radiation oncologists. The stricter criterion for the CTV_{70} relates to the higher recurrence rate observed in this region [33,39,40].

The sCTs were validated against dose calculations in [36]. To validate the use of propagated CTV on the sCTs for further analysis, 748 auto-propagated CTV contours on the daily sCTs (Fig. 1b) for the first 11 out of 28 patients were reviewed and corrected by the same HNC radiation oncologist (EO) following clinical delineation guidelines (e.g. [41]) on the sCTs. Although anatomical landmarks were more visible on the sCT and that the sCT presents information in a way more familiar to the radiation oncologist compared with the CBCT, it is still insufficient to redraw the GTV everywhere just using the sCTs, even so for the diagnostic CT without contrast. The contours of the propagated CTVs on the sCTs were therefore evaluated and adjusted based partially on the GTV on the planning CT, PET and MRI scans, similar to clinical practice. The GTV contours of clinically adapted plans were also considered in the evaluation to evaluate subsequent CTVs. The corrected CTV_{70} and $CTV_{54.25}$ are denoted as physician corrected CTV_{70} and physician corrected $CTV_{54.25}$, respectively. Although inter-observer variability [42] is absent, intra-observer variability persisted due to the

lack of ground truth and the difficulty in assessing each CT slice independently [43]. With strict and consistent adherence to delineation guidelines, this variability reduces and becomes clinically irrelevant [44]. Given that no consensus exists on evaluating the propagated contours [11,45], the accuracy of the propagated CTVs was determined against the physician corrected CTVs based on the residual geometrical error dr and the dice similarity coefficient (DSC). The residual geometrical errors dr for physician corrected CTVs were similarly determined, but by replacing the propagated CTV with the physician corrected CTV in Fig. 1b. The volumetric DSC was compared using:

$$\Delta DSC_{mean} = \frac{1}{n}\sum_{i=1}^{i=n}\Delta DSC_i \qquad (1)$$

where,

$$\Delta DSC_i = \frac{1}{N}\sum_{j=1}^{j=N}\Big(DSC(\text{propagated CTV, nominal plan CTV})_{ij}$$
$$-DSC(\text{physician corrected CTV, nominal plan CTV})_{ij}\Big).$$

Quantities N = 11 and n = 31 are the number of patients and available sCTs, respectively, with all patients having at least 31 scans.

Upon determining the accuracy of the propagated CTVs contours with the physician corrected CTVs for 11 patients, the residual geometrical error dr was computed using the propagated CTVs for the CTV_{70} and $CTV_{54.25}$ for the entire patient cohort with 952 sCT scans. For the $CTV_{54.25}$, the nodes above level III extends down to the level of the shoulders. Given the high shoulder position variability [46], the residual geometrical error dr($CTV_{54.25}$) in regions superior and inferior to the cricoid cartilage was separately determined and subsequently compared. For the CTV_{70}, the analysis was excluded as on average, only 4.2% of the target volume lies inferior to the cricoid for our study cohort.

Dosimetric and TCP analysis

To investigate how the delivered target dose coverage and the TCP are impacted by the residual geometrical errors dr, the accumulated doses were computed using the clinical (original and adapted) plans for each patient [25,47]. These nominal treatment plans were robustly optimized with 3 mm/3% setup and range uncertainty settings based on the robust optimization and evaluation approach of the Dutch consensus for proton therapy centers [48]. Doses were recalculated on the daily sCTs based on original or adapted treatment plans. The sCT doses were then warped using DIR and accumulated on the original CT.
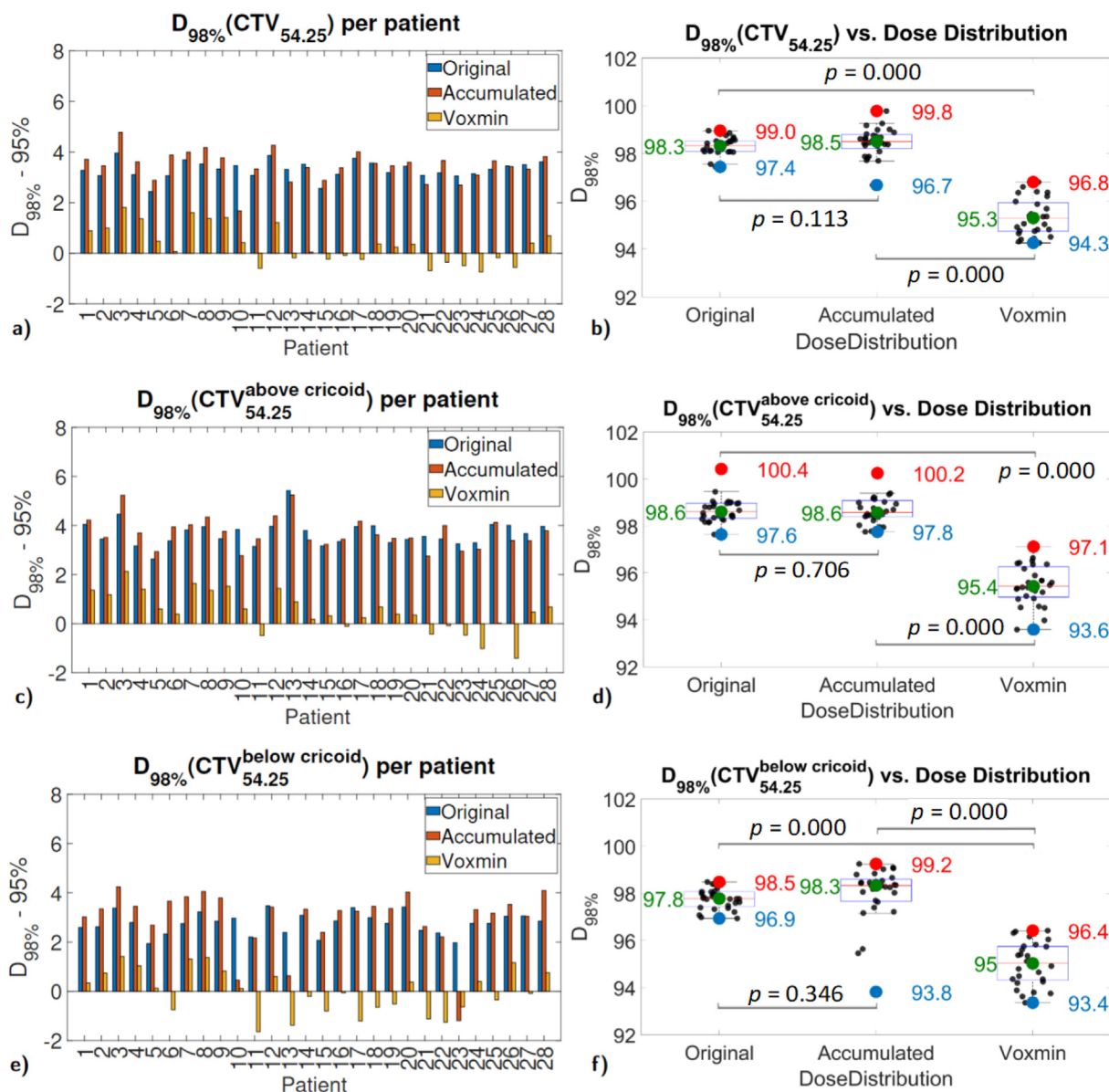
Fig. 5. Dose coverage displayed as the difference between the $D_{98\%}$ and 95% of the prescription dose for (a) $CTV_{54.25}$, (c) $CTV_{54.25}$ above the cricoid and (e) $CTV_{54.25}$ below the cricoid. The corresponding CTV $D_{98\%}$ coverages for all patients are plotted against different dose distributions in figures (b), (d) and (f), respectively.

For target dose coverage impact, D98 was compared between the accumulated, original, and voxel-wise minimum (voxmin) dose distributions for both CTV_{70} and $CTV_{54.25}$. The voxmin dose distributions were obtained by simulating 14 setup error scenarios for two density shifts of +/-3% for the original plan per patient [48]. The voxmin dose distribution is then derived from the minimum dose per voxel across all scenarios. In our clinical practice, target coverage is considered adequate when D98 > 95% for the voxmin dose distribution. For the $CTV_{54.25}$, regions above and below the cricoid cartilage were also compared.

Tumor control probability (TCP) was determined from the method of Luhr [33], based on the DVH in the three sub-volumes of the target: 1) the gross tumor volume (GTV), 2) the CTV_{70} excluding the GTV and 3) the $CTV_{54.25}$ excluding the CTV_{70}. The influence of underdosage of the subvolumes to the TCP is a function of the rate of recurrences in those volumes. The required input TCP parameters (dose at 50% tumor control D_{50} and normalized slope γ_{50}) for HNC were taken from [25], with recurrences of 82%, 16% and 2% for the GTV, the remaining CTV_{70} and the remaining $CTV_{54.25}$, respectively [39].

The mean of the TCP for the accumulated doses was tested for statistical significance against the original and voxmin doses using the two-tailed paired-sample t-test. Statistical significance was set at $p < \alpha/2$, with significance level $\alpha = 0.05$.

Results

For the CTV_{70}, the residual geometrical error dr was found to be 1.70 and 1.86 mm for the physician corrected CTV and propagated CTV, respectively. For the $CTV_{54.25}$, the residual geometrical error dr for the physician corrected CTV and propagated CTV contours was 2.35 and 2.61 mm, respectively. The differences in the error were less than 0.3 mm. The absolute value of ΔDSC between the propagated CTVs and physician corrected CTVs averaged over 11 patients (Eq. (1)) was smaller than 1.8% for both CTV_{70} and $CTV_{54.25}$ for all treatment fractions. The obtained ΔDSC_{mean} was − 0.45% and − 0.82% for CTV_{70} and $CTV_{54.25}$, respectively, indicating minor differences between the physician corrected CTV and propagated CTV contours. The results were consistent with earlier

studies that found subvoxel accuracy of the deformable image registration of Raystation at the head and neck regions [49,50].

Next, the residual geometrical error dr was determined for the entire patient cohort. Fig. 2 shows the percentage of daily CTVs against the expansion of the nominal plan CTV for CTV_{70} (Fig. 2a) and $CTV_{54.25}$ (Fig. 2b). The $CTV_{54.25}$ regions above and below the cricoid cartilage are shown in Fig. 2c and Fig. 2d, respectively. For the entire patient cohort, the residual geometrical error dr was 1.91 and 1.90 mm for the CTV_{70} and $CTV_{54.25}$, respectively. Patient 10 had the largest residual geometrical error dr of 3.72 mm for the $CTV_{54.25}$. However, below the cricoid cartilage, the residual geometrical error dr (3.93 mm, range, 0.97 mm to 8.49 mm) was almost four times larger than above the cricoid cartilage (dr = 1 mm; range, 0.15 mm to 2.13 mm). Patients 7, 10, 13 and 23 (oral cavity, nasopharyngeal, oropharyngeal and nasal cavity carcinomas, respectively) had substantially larger errors compared with the rest of the cohort, with patient 23 having the largest error at 8.49 mm. Fig. 3 shows a sCT scan fused with the nominal plan CT for patients 10 and 23. Clearly, the majority of errors occurred in the $CTV_{54.25}$ region below the cricoid cartilage, whereas the match was almost perfect within 1 mm in the head and upper neck region.

The calculated TCP values are presented against the original, accumulated and voxmin dose distributions in Fig. 4 for all 28 patients. The TCP of the accumulated dose was statistically similar to the TCP of the original dose, whereas the TCP of the voxmin dose was significantly lower. Clearly, the TCP is unaffected by the large residual errors of the $CTV_{54.25}$ observed below the cricoid cartilage.

Fig. 5 shows the dose coverage of the entire $CTV_{54.25}$ and the $CTV_{54.25}$ above and below the cricoid cartilage for each patient (Fig. 5a, c, e) and against the dose distributions (Fig. 5b, d, f). Patient 10 had the lowest $CTV_{54.25}$ coverage, which corresponds to largest residual geometrical error dr for the $CTV_{54.25}$ (Fig. 2b). All regions met the target coverage except for the $CTV_{54.25}$ below the cricoid cartilage for patient 23, with a dose coverage of $D_{98\%}$ = 93.8%, even lower than the voxmin dose coverage. This patient had also the largest residual geometrical error dr observed for the $CTV_{54.25}$ below the cricoid cartilage (Fig. 2d). However, the impact on the coverage of the entire $CTV_{54.25}$ is negligible. The dose coverage for all prophylactic CTV regions is also statistically similar between the original and accumulated dose distributions.

Discussion

In this study, we have attempted to quantify the accuracy of the propagated contours by having a physician performed manual review. Results show minimal differences in the geometrical errors obtained between the propagated CTVs and the physician corrected CTVs. The accuracy of the deformable image registration algorithm used in this study was shown earlier to be up to 2 mm [50]. Although we do not expect the uncertainty by deformable image registration to impact our main findings, it is important to note that our analysis is fundamentally limited by the available information in a CBCT, hence the corrected sCT. As a result, the physician's review on the sCT serves only as a surrogate for true accuracy. Assessing this accuracy is extremely challenging and falls outside the scope of this work. Nonetheless, as radiotherapy progresses into an era of online or real-time adaption, it remains vital to be aware of this inherent limitation.

Residual geometrical errors are found to be less than 2 mm for both the CTV_{70} and $CTV_{54.25}$ after daily online CBCT verification. However, the $CTV_{54.25}$ error has a larger spread attributed to the higher lower neck and shoulder position variability, independent of the primary tumor type (3.93 mm for lower neck and shoulder c.f. 1.00 mm for head and upper neck). Large residual deformation

errors of more than 3 mm of the CTVs in the lower neck are also found by several studies [24,51,52], suggesting the use of larger margins for lower neck targets, particularly targets involving the larynx. Recent studies showed that a dose coverage of 40 Gy could be adequate for the prophylactic CTV [53,54], suggesting that current CTV underdosage due to large errors might be clinically irrelevant. However, the geometrical errors of the lower neck and shoulders should not be disregarded and should be properly accounted for during treatment planning, especially when dose is de-escalated for the prophylactic CTV. This will also avoid unexpected high doses to the surrounding healthy tissues.

Our results also show that the large residual geometrical errors observed in the neck and shoulder regions does not necessary lead to underdosage to the $CTV_{54.25}$ over the course of treatment. One patient in our study had a slight underdosage of the $CTV_{54.25}$ in the lower neck regions even though 8 mm residual geometrical errors were present. This is similarly observed by Hamming-Vrieze et al. [11] and Van Kranen et. al [24], where gross anatomical changes and the calculated dosimetric differences appear weakly correlated.

For all patients in our cohort, the TCP of both the original and accumulated dose distributions is higher than the TCP of the voxmin dose distribution, or the lower limit of the TCP value for which we still consider adequate for our treatments. The TCP calculated according to Luhr et al. in our study is subsequently found relatively insensitive to the underdosage of the $CTV_{54.25}$ compared with that of the CTV_{70}. From empirical data, most recurrences occur in the GTV. Therefore, the TCP obtained from the accumulated dose is not severely affected by the lower doses to the $CTV_{54.25}$ regions observed for some patients in this study. However, the ΔTCP due to residual geometrical errors may differ per tumor site despite similar tumor stages and volumes (e.g., HPV-positive and HPV-negative oropharyngeal cancers). Also, the impact of the large lower neck geometrical errors on the TCP of tumors located at the lower neck regions is expected to be larger. Therefore, the large positioning errors of the lower neck and shoulders have to be considered in treatment planning.

A limitation of our study is that our cohort did not contain a lot of supraglottic laryngeal cancer patients treated. The consequences of the larger lower neck geometrical errors for TCP might be more for patients with laryngeal cancers or with positive nodes in level II or higher due to the higher risk of nodal metastases in this region (level III and IV). Consequently, asymmetrical CMRO setup error margins for the head and upper neck regions at 2 mm and lower neck regions at 4 mm may be considered if target volume dose coverage to the lower neck regions is critical, taking in account the a priori risks of nodal metastases and recurrences in these areas.

We recognize that accurate recording of the GTV and CTV on a CT without contrast (hence on our daily synthetic CTs) is not always possible. This uncertainty may influence inter- and intraobserver variability and hence the validation of our propagated contours. However, the correction of the propagated contours by our radiation oncologist in this study was carried out following clinical practice and strict delineation guidelines. Our conclusions are therefore expected not to be greatly affected.

Another limitation is that the isocentric errors of the onboard CBCT imaging system and the delivery beam are neglected. From the results obtained from our comprehensive machine QA program in an earlier work, the total isocentricity error is conservatively estimated at 0.50 mm [25]: the interfraction geometrical errors are still much larger. Our conclusions are therefore expected not to change. The limited FoV of the CBCTs could also impact the accuracy of the contour propagation and dose reconstructions of the CTVs. However, the CTVs are usually far from the FoV edges and therefore the study outcome is expected not to change.

The large geometrical errors at the shoulder regions observed in our study could be attributed to the immobilization device we used. We noticed our masks were more compliant at the shoulder regions due to more material stretching. Using a more rigid, immobilization mask may mitigate this issue. However, this tend to decrease the comfort of the patients, hence increasing positioning difficultly, which should be taken into consideration.

It should be noted that the errors obtained in this study are derived assuming negligible intrafraction motions due to e.g., swallowing or large tongue displacements. Care should be taken when applying a 2 mm margin for a patient who swallows frequently, especially for IMPT treatments with no repainting as the pencil beam spots could miss the target completely, increasing the interplay effect. Intrafraction motion could also be important for treatment plans having short irradiation times. Online or real time plan adaption or motion intervention strategies [55] may be considered for these patients.

In this study, we investigated how all errors impact the choice of robust optimization settings. An important follow up would be to differentiate the nature of the geometrical errors and investigate techniques to mitigate the respective errors. As Korevaar et al. [48] have earlier demonstrated, the evaluation of the voxmin CTV-based plan evaluation is an alternative to PTV-based plan evaluation. We expect our conclusions on the margins to hold also for the PTV-method. This investigation, which is outside the scope of our study, would be an interesting follow up.

Conclusion

Our analysis on 952 daily sCTs indicates that the reduction of CMRO setup uncertainty settings from 3 mm to 2 mm for robust planning of HNC IMPT patients is acceptable for the general population for both therapeutic and prophylactic CTVs above the cricoid cartilage to account for the residual geometrical errors. The range uncertainty is considered 3%. Treatment setup conditions include employment of a 5-point immobilization mask, bite block or tongue depressor for oral cavity tumors and 6D couch in conjunction with daily 3D online verification. This is consistent with the findings presented by Wagenaar et al using probabilistic dose accumulation. Caution should be taken when applying this 2 mm margin below the cricoid cartilage on patients with large irregular head and neck motions, with primary tumors or high nodal metastases risk in the neck and shoulder regions or when using immobilization devices where the shoulders are less reproducible. Asymmetrical patient and location specific margins could be considered during treatment planning: 2 mm at the head and upper neck regions and 4 mm at the lower neck and shoulder regions. Online or real time adaptive radiotherapy, better, possibly more rigid (depending on patient comfort) immobilization devices or motion management strategies could also be considered to reduce the lower neck and shoulder residual geometrical errors. The results are also expected to translate to HNC patients receiving photon or electron radiotherapy with similar immobilization and treatment setup verification.

Funding

CRediT authorship contribution statement

Kelvin Ng Wei Siang: Conceptualization, Project administration, Data curation, Methodology, Investigation, Software, Visualization, Formal analysis, Writing – original draft. **Stefan Both:** Conceptualization, Supervision, Resources, Project administration, Writing – review & editing. **Edwin Oldehinkel:** Data curation, Resources, Writing – review & editing. **Johannes A. Langendijk:** Resources, Writing – review & editing. **Dirk Wagenaar:** Conceptualization, Supervision, Resources, Writing – review & editing.

Declaration of Competing Interest

The authors declare that they have no known competing financial interests or personal relationships that could have appeared to influence the work reported in this paper.

Appendix A. Supplementary material

Supplementary data to this article can be found online at https://doi.org/10.1016/j.radonc.2023.109856.

References

[1] Strom T, Naghavi AO, Messina JL, Kim S, Torres-Roca JF, Russell J, et al. Improved local and regional control with radiotherapy for Merkel cell carcinoma of the head and neck. Head Neck Jan 2017;39:48–55. https://doi.org/10.1002/hed.24527. ISSN 10970347.

[2] Schüttrumpf L, Marschner S, Scheu K, Hess J, Rietzler S, Walch A, et al. Definitive chemoradiotherapy in patients with squamous cell cancers of the head and neck - Results from an unselected cohort of the clinical cooperation group "personalized Radiotherapy in Head and Neck Cancer". Radiat Oncol Jan 2020;15:1–12. https://doi.org/10.1186/s13014-019-1452-4. ISSN 1748717X.

[3] Benjamin Lacas, Jean Bourhis, Jens Overgaard, Qiang Zhang, Vincent Grégoire, Matthew Nankivell, Björn Zackrisson, Zbigniew Szutkowski, Rafal Suwinski, Michael Poulsen, Brian O'Sullivan, Renzo Corvò, Sarbani Ghosh Laskar, Carlo Fallai, Hideya Yamazaki, Werner Dobrowsky, Kwan Ho Cho, Adam S Garden, Johannes A Langendijk, Celia Maria Pais Viegas, John Hay, Mohamed Lotayef, Mahesh K.B. Parmar, Anne Aupérin, Carla van Herpen, Philippe Maingon, Andy M Trotti, Cai Grau, Jean Pierre Pignon, Pierre Blanchard, Jacques Bernier, Quynh Thu Le, Andy Trotti, Jai Prakash Agarwal, Kian K. Ang, Hassan K. Awwad, Almalina Bacigalupo, Harry Bartelink, Ellen Benhamou, Wilfried Budach, Imjai Chitapanarux, Laurence Collette, Carla Dani, Stanley Dische, James W. Denham, Chantal ML Driessen, Sushmita Ghoshal, Vincent Gregoire, John H. Hay, Andrzej Hliniak, Jørgen Johansen, Claus Andrup Kristiansen, Valentina Krstevska, Michel Lapeyre, Boguslaw Maciejewski, Wojciech Michalski, Sung Ho Moon, Per Nilsson, Patrizia Olmi, Kinji Nishiyama, Michael G. Poulsen, Kunnambath Ramadas, Anupam Rishi, David I. Rosenthal, Giuseppe Sanguineti, Michele I. Saunders, Christian Sire, Krzysztof Skladowski, Luis Souhami, Nitin Tandon, Harm van Tinteren, Valter Torri, Lee Tripcony, John Waldron, Joachim Widder, Stuart Wong, and Jonn S. Wu. Role of radiotherapy fractionation in head and neck cancers (MARCH): an updated meta-analysis. The Lancet Oncology, 18:1221–1237, 2017. ISSN 14745488. doi: 10.1016/S1470-2045(17)30458-8.

[4] Johansen S, Norman MH, Dale E, Amdal CD, Furre T, Malinen E, et al. Patterns of localregional recurrence after conformal and intensity-modulated radiotherapy for head and neck cancer. Radiat Oncol 2017;12:1. https://doi.org/10.1186/s13014-017-0829-5. ISSN 1748717X.

[5] Van Herk M. Errors and margins in radiotherapy. Semin Radiat Oncol 2004;14:52–64. https://doi.org/10.1053/j.semradonc.2003.10.003. ISSN 10534296.

[6] Kraan AC, Van De Water S, Teguh DN, Al-Mamgani A, Madden T, Kooy HM, et al. Dose uncertainties in IMPT for oropharyngeal cancer in the presence of anatomical, range, and setup errors. Int J Radiat Oncol Biol Phys 2013;87:888–96. https://doi.org/10.1016/j.ijrobp.2013.09.014. ISSN 03603016.

[7] Djordjevic M, Sjöholm E, Tullgren O, Sorcini B. Assessment of residual setup errors for anatomical sub-structures in image-guided head-And-neck cancer radiotherapy. Acta Oncol 2014;53:646–53. https://doi.org/10.3109/0284186X.2013.862593. ISSN 1651226X.

[8] Razek MA, Elshahat K, Khalil E, Khalil W, Allouche F. Dosimetric evaluation of patient setup errors due to uncertainties during imrt for head and neck cancer cases. Onkol Radioter 2021;15:19–28. ISSN 24499161.

[9] Bruijnen T, Stemkens B, Terhaard CHJ, Lagendijk JJW, Raaijmakers CPJ, Tijssen RHN. Intrafraction motion quantification and planning target volume margin determination of head-and-neck tumors using cine magnetic resonance imaging. Radiother Oncol 2019;130:82–8. https://doi.org/10.1016/j.radonc.2018.09.015. ISSN 18790887.

[10] van Beek S, Jonker M, Hamming-Vrieze O, Al-Mamgani A, Navran A, Remeijer P, et al. Protocolised way to cope with anatomical changes in head neck cancer during the course of radiotherapy. Tech Innov Patient Support Radiat Oncol 2019;12:34–40. https://doi.org/10.1016/j.tipsro.2019.11.001. ISSN 24056324.

[11] Hamming-Vrieze O, van Kranen S, Walraven I, Navran A, Al-Mamgani A, Tesselaar M, et al. Deterioration of intended target volume radiation dose due

to anatomical changes in patients with head-and-neck cancer. Cancers sep 2021;13. https://doi.org/10.3390/cancers13174253. ISSN 20726694.

[12] Gurney-Champion OJ, McQuaid D, Dunlop A, Wong KH, Welsh LC, Riddell AM, et al. MRI-based assessment of 3D intrafractional motion of head and neck cancer for radiation therapy. Int J Radiat Oncol Biol Phys Feb 2018;100:306–16. https://doi.org/10.1016/j.ijrobp.2017.10.016. ISSN 1879355X.

[13] Bradley JA, Paulson ES, Ahunbay E, Christopher Schultz X, Li A, Wang D. Dynamic MRI analysis of tumor and organ motion during rest and deglutition and margin assessment for radiotherapy of head-and-neck cancer. Int J Radiat Oncol Biol Phys Dec 2011;81:e803–12. https://doi.org/10.1016/j.ijrobp.2010.12.015. ISSN 03603016.

[14] Van Herk M, Remeijer P, Rasch C, Lebesque JV. The probability of correct target dosage: Dose-population histograms for deriving treatment margins in radiotherapy. Int J Radiat Oncol Biol Phys 2000;47:1121–35. https://doi.org/10.1016/S0360-3016(00)00518-6. ISSN 03603016.

[15] V. Grégoire and T. R. Mackie. State of the art on dose prescription, reporting and recording in Intensity-Modulated Radiation Therapy (ICRU report No. 83). Cancer/Radiotherapie, 15:555–559, 2011. ISSN 12783218. doi: 10.1016/j.canrad.2011.04.003.

[16] Van Der Voort S, Van De Water S, Perkó Z, Heijmen B, Lathouwers D, Hoogeman M. Robustness recipes for minimax robust optimization in intensity modulated proton therapy for oropharyngeal cancer patients. Int J Radiat Oncol Biol Phys 2016;95:163–70. https://doi.org/10.1016/j.ijrobp.2016.02.035. ISSN 1879355X.

[17] Unkelbach J, Alber M, Bangert M, Bokrantz R, Chan TCY, Deasy JO, et al. Robust radiotherapy planning. Phys Med Biol 2018;63. https://doi.org/10.1088/1361-6560/aae659. ISSN 13616560.

[18] Dirk Wagenaar, Roel G.J. Kierkels, Jeffrey Free, Johannes A. Langendijk, Stefan Both, and Erik W. Korevaar. Composite minimax robust optimization of VMAT improves target coverage and reduces non-target dose in head and neck cancer patients. Radiotherapy and Oncology, 136:71–77, jul 2019. ISSN 18790887. doi: 10.1016/j.radonc.2019.03.019.

[19] Biston MC, Chiavassa S, Grégoire V, Thariat J, Lacornerie T. Time of PTV is ending, robust optimization comes next. Cancer/Radiotherapie 2020;24:676–86. https://doi.org/10.1016/j.canrad.2020.06.016. ISSN 17696658.

[20] D Maleike, J Unkelbach, and U Oelfke. Simulation and visualization of dose uncertainties due to interfractional organ motion. Physics in Medicine and Biology, 51:2237–2252, 2006. ISSN 00319155. doi: 10.1088/0031-9155/51/9/009.

[21] Chen W, Unkelbach J, Trofimov A, Madden T, Kooy H, Bortfeld T, et al. Including robustness in multicriteria optimization for intensity-modulated proton therapy. Phys Med Biol Feb 2012;57:591–608. https://doi.org/10.1088/0031-9155/57/3/591. ISSN 00319155.

[22] Steven van de Water, Iris van Dam, Dennis R. Schaart, Abrahim Al-Mamgani, Ben J.M. Heijmen, and Mischa S. Hoogeman. The price of robustness; impact of worst-case optimization on organ-at-risk dose and complication probability in intensity-modulated proton therapy for oropharyngeal cancer patients. Radiotherapy and Oncology, 120:56–62, jul 2016. ISSN 18790887. doi: 10.1016/j.radonc.2016.04.038.

[23] Lalonde A, Bobić M, Winey B, Verburg J, Sharp GC, Paganetti H. Anatomic changes in head and neck intensity-modulated proton therapy: Comparison between robust optimization and online adaptation. Radiother Oncol jun 2021;159:39–47. https://doi.org/10.1016/j.radonc.2021.03.008. ISSN 18790887.

[24] Simon van Kranen, Olga Hamming-Vrieze, Annelisa Wolf, Eugène Damen, Marcel van Herk, and Jan Jakob Sonke. Head and Neck Margin Reduction With Adaptive Radiation Therapy: Robustness of Treatment Plans Against Anatomy Changes. International Journal of Radiation Oncology Biology Physics, 96:653–660, 2016. ISSN 1879355X. doi: 10.1016/j.ijrobp.2016.07.011.

[25] Dirk Wagenaar, Roel G.J. Kierkels, Arjen van der Schaaf, Arturs Meijers, Daniel Scandurra, Nanna M. Sijtsema, Erik W. Korevaar, Roel J.H.M. Steenbakkers, Antje C. Knopf, Johannes A. Langendijk, and Stefan Both. Head and neck IMPT probabilistic dose accumulation: Feasibility of a 2 mm setup uncertainty setting. Radiotherapy and Oncology, 154:45–52, 2021. ISSN 18790887. doi: 10.1016/j.radonc.2020.09.001.

[26] Miura H, Ozawa S, Nagata Y. Efficacy of robust optimization plan with partial-arc VMAT for photon volumetricmodulated arc therapy: A phantom study. J Appl Clin Med Phys sep 2017;18:97–103. https://doi.org/10.1002/acm2.12131. ISSN 15269914.

[27] Jesús Rojo-Santiago, Steven J.M. Habraken, Danny Lathouwers, Alejandra Méndez Romero, Zoltán Perkó and Mischa S. Hoogeman. Accurate assessment of a Dutch practical robustness evaluation protocol in clinical PT with pencil beam scanning for neurological tumors. Radiotherapy and Oncology, 163:121–127, 2021. ISSN 18790887. doi: 10.1016/j.radonc.2021.07.028.

[28] Abrahim Al-Mamgani, Rob Kessels, Tomas Janssen, Arash Navran, Suzanne van Beek, Casper Carbaat, Willem H. Schreuder, Jan Jakob Sonke, and Corrie A.M. Marijnen. The dosimetric and clinical advantages of the GTV-CTV-PTV margins reduction by 6 mm in head and neck squamous cell carcinoma: Significant acute and late toxicity reduction. Radiotherapy and Oncology, 168:16–22, 2022. ISSN 18790887. doi: 10.1016/j.radonc.2022.01.013.

[29] Tilly D, Ahnesjö A. Fast dose algorithm for generation of dose coverage probability for robustness analysis of fractionated radiotherapy. Phys Med Biol jun 2015;60:5439–54. https://doi.org/10.1088/0031-9155/60/14/5439. ISSN 13616560.

[30] Zhiyong Yang, Xiaodong Zhang, Xianliang Wang, X. Ronald Zhu, Brandon Gunn, Steven J. Frank, Yu Chang, Qin Li, Kunyu Yang, Gang Wu, Li Liao, Yupeng Li, Mei Chen, and Heng Li. Multiple-CT optimization: An adaptive optimization method to account for anatomical changes in intensity-modulated proton therapy for head and neck cancers. Radiotherapy and Oncology, 142:124–132, jan 2020. ISSN 18790887. doi: 10.1016/j.radonc.2019.09.010.

[31] Cubillos-Mesías M, Troost EGC, Lohaus F, Agolli L, Rehm M, Richter C, et al. Quantification of plan robustness against different uncertainty sources for classical and anatomical robust optimized treatment plans in head and neck cancer proton therapy. Br. J. Radiol. Mar 2020;93. https://doi.org/10.1259/bjr.20190573. ISSN 1748880X.

[32] Stroom JC, Heijmen BJM. Geometrical uncertainties, radiotherapy planning margins, and the ICRU-62 report. Radiother Oncol 2002;64:75–83. https://doi.org/10.1016/S0167-8140(02)00140-8.

[33] Armin Lühr, Steffen Löck, Annika Jakobi, Kristin Stützer, Anna Bandurska-Luque, Ivan Richter Vogelius, Wolfgang Enghardt, Michael Baumann, and Mechthild Krause. Modeling tumor control probability for spatially inhomogeneous risk of failure based on clinical outcome data. Zeitschrift fur Medizinische Physik, 27:285–299, 2017. ISSN 18764436. doi: 10.1016/j.zemedi.2017.06.003.

[34] Fracchiolla F, Fellin F, Innocenzi M, Lipparini M, Lorentini S, Widesott L, et al. A pre-absorber optimization technique for pencil beam scanning proton therapy treatments. Phys Med 2019;57:145–52. https://doi.org/10.1016/j.ejmp.2018.12.014. ISSN 1724191X.

[35] Veiga C, McClelland J, Moinuddin S, Lourenço A, Ricketts K, Annkah J, et al. Toward adaptive radiotherapy for head and neck patients: Feasibility study on using CT-to-CBCT deformable registration for "dose of the day" calculations. Med Phys Mar 2014;41:. https://doi.org/10.1118/14864240. ISSN 00942405031703.

[36] Thummerer A, Zaffino P, Meijers A, Marmitt GG, Seco J, Steenbakkers RJHM, et al. Comparison of CBCT based synthetic CT methods suitable for proton dose calculations in adaptive proton therapy. Phys Med Biol 2020;65. https://doi.org/10.1088/1361-6560/ab7d54. ISSN 13616560.

[37] Ola Weistrand and Stina Svensson. The ANACONDA algorithm for deformable image registration in radiotherapy. Medical Physics, 42: 40–53, 2015. ISSN 00942405. doi: 10.1118/1.4894702.

[38] La Macchia M, Fellin F, Amichetti M, Cianchetti M, Gianolini S, Paola V, et al. Systematic evaluation of three different commercial software solutions for automatic segmentation for adaptive therapy in head-and-neck, prostate and pleural cancer. Radiat Oncol sep 2012;7. https://doi.org/10.1186/1748-717X-7-160. ISSN 1748717X.

[39] Anne K. Due, Ivan R. Vogelius, Marianne C. Aznar, Søren M. Bentzen, Anne K. Berthelsen, Stine S. Korreman, Annika Loft, Claus A. Kristensen, and Lena Specht. Recurrences after intensity modulated radiotherapy for head and neck squamous cell carcinoma more likely to originate from regions with high baseline [18F]-FDG uptake. Radiotherapy and Oncology, 111:360–365, 2014. ISSN 18790887. doi: 10.1016/j.radonc.2014.06.001.

[40] Ruta Zukauskaite, Christian R. Hansen, Cai Grau, Eva Samsøe, Jørgen Johansen, Jørgen B.B. Petersen, Elo Andersen, Carsten Brink, Jens Overgaard, and Jesper G. Eriksen. Local recurrences after curative IMRT for HNSCC: Effect of different GTV to high-dose CTV margins. Radiotherapy and Oncology, 126:48–55, jan 2018. ISSN 18790887. doi: 10.1016/j.radonc.2017.11.024.

[41] Vincent Grégoire, Kian Ang, Wilfried Budach, Cai Grau, Marc Hamoir, Johannes A. Langendijk, Anne Lee, Quynh Thu Le, Philippe Maingon, Chris Nutting, Brian O'Sullivan, Sandro V. Porceddu, and Benoit Lengele. Delineation of the neck node levels for head and neck tumors: A2013 update. DAHANCA, EORTC, HKNPCSG, NCIC CTG, NCRI, RTOG, TROG consensus guidelines. Radiotherapy and Oncology, 110 :172–181, 2014. ISSN 18790887. doi: 10.1016/j.radonc.2013.10.010.

[42] van der Veen J, Gulyban A, Nuyts S. Interobserver variability in delineation of target volumes in head and neck cancer. Radiother Oncol 2019;137:9–15. https://doi.org/10.1016/j.radonc.2019.04.006. ISSN 18790887.

[43] Eric L.H. Khoo, Karlissa Schick, Ashley W. Plank, Michael Poulsen, Winnie W.G. Wong, Mark Middleton, and Jarad M. Martin. Prostate contouring variation: Can it be fixed? International Journal of Radiation Oncology Biology Physics, 82:1923–1929, apr 2012. ISSN 03603016. doi: 10.1016/j.ijrobp.2011.02.050.

[44] Pete Bridge, Andrew Fielding, Pamela Rowntree, and Andrew Pullar. Intraobserver Variability: Should We Worry?, sep 2016. ISSN 18767982.

[45] Michael V. Sherer, Diana Lin, Sharif Elguindi, Simon Duke, Li Tee Tan, Jon Cacicedo, Max Dahele, and Erin F. Gillespie. Metrics to evaluate the performance of auto-segmentation for radiation treatment planning: A critical review, jul 2021. ISSN 18790887.

[46] Asma Sarwar, Shelly English, Yanni Papastavrou, and Anna Thompson. Impact of brachial plexus movement during radical radiotherapy for head and neck cancers: The case for a larger planning organ at risk volume margin. Journal of Radiotherapy in Practice, 19:103–107, jun 2020. ISSN 14671131. doi: 10.1017/S1460396919000499.

[47] Arturs Meijers, Gabriel Guterres Marmitt, Kelvin Ng Wei Siang, Arjen van der Schaaf, Antje C. Knopf, Johannes A. Langendijk, and Stefan Both. Feasibility of patient specific quality assurance for proton therapy based on independent dose calculation and predicted outcomes. Radiotherapy and Oncology, 150:136–141, sep 2020. ISSN 18790887. doi: 10.1016/j.radonc.2020.06.027.

[48] Korevaar, E. W., Habraken, S. J. M., Scandurra, D., Kierkels, R. G. J., Unipan, M., Eenink, M. G. C., Steenbakkers, R. J. H. M., Peeters, S. G., Zindler, J. D., Hoogeman, M., & Langendijk, J. A. (2019). Practical robustness evaluation in

radiotherapy-A photon and proton-proof alternative to PTV-based plan evaluation. https://doi.org/10.1016/j.radonc.2019.08.005.

[49] Gianfranco Loi, Marco Fusella, Eleonora Lanzi, Elisabetta Cagni, Cristina Garibaldi, Giuseppina Iacoviello, Francesco Lucio, Enrico Menghi, Roberto Miceli, Lucia C. Orlandini, Antonella Roggio, Federica Rosica, Michele Stasi, Lidia Strigari, Silvia Strolin, and Christian Fiandra. Performance of commercially available deformable image registration platforms for contour propagation using patient-based computational phantoms: A multi-institutional study: A. Medical Physics, 45:748–757, feb 2018. ISSN 00942405. doi: 10.1002/mp.12737.

[50] Rafael García-Mollá, Noelia de Marco-Blancas, Jorge Bonaque, Laura Vidueira, Juan López-Tarjuelo, and José Perez-Calatayud. Validation of a deformable image registration produced by a commercial treatment planning system in head and neck. Physica Medica, 31:219–223, may 2015. ISSN 1724191X. doi: 10.1016/j.ejmp.2015.01.007.

[51] Charles A. Baron, Musaddiq J. Awan, Abdallah S. R. Mohamed, Imad Akel, David I. Rosenthal, G. Brandon Gunn, Adam S. Garden, Brandon A. Dyer, Laurence Court, Parag R. Sevak, Esengul Kocak-Uzel, and Clifton D. Fuller. Estimation of daily interfractional larynx residual setup error after isocentric alignment for head and neck radiotherapy: Quality assurance implications for target volume and organs-at-risk margination using daily CT on-rails imaging. Journal of Applied Clinical Medical Physics, 16:159–169, 2015. ISSN 15269914. doi: 10.1120/jacmp. v16i1.5108.

[52] Biau J, Pointreau Y, Blanchard P, Khampan C, Giraud P, Lapeyre M, et al. Radiotherapy for laryngeal cancers. Cancer/Radiother Feb 2022;26:206–12. https://doi.org/10.1016/j.canrad.2021.09.004. ISSN 17696658.

[53] Daan Nevens, Fréderic Duprez, Jean François Daisne, Julie Schatteman, Aline Van der Vorst, Wilfried De Neve, and Sandra Nuyts. Recurrence patterns after a decreased dose of 40 Gy to the elective treated neck in head and neck cancer. Radiotherapy and Oncology, 123:419–423, 2017. ISSN 18790887. doi: 10.1016/j.radonc.2017.03.003.

[54] David J. Thomson. Reduced Dose and Volume Elective Nodal Radiation Therapy for Head and Neck Cancer: Challenging the Paradigm. International Journal of Radiation Oncology Biology Physics, 109:941–943, 2021. ISSN 1879355X. doi: 10.1016/j.ijrobp.2020.11.018.

[55] Vincent W.C. Wu, Amanda P.L. Ng, and Emily K.W. Cheung. Intrafractional motion management in external beam radiotherapy. Journal of X-Ray Science and Technology, 27:1071–1086, 2020. ISSN 08953996. doi: 10.3233/XST-180472.